Kinetics of high-temperature oxidation of (Ti,Ta)(C,N)-based cermets

3 AUTHORS:

Ernesto Chicardi
Universidad Técnica Federico Santa María
24 PUBLICATIONS **108** CITATIONS

SEE PROFILE

J. M. Córdoba
Universidad de Sevilla
63 PUBLICATIONS **516** CITATIONS

SEE PROFILE

Francisco J. Gotor
Spanish National Research Council
109 PUBLICATIONS **1,540** CITATIONS

SEE PROFILE

Kinetics of high-temperature oxidation of (Ti,Ta)(CN)-based cermets

E. Chicardi*[1,2], J. M. Córdoba[1,3] and F. J. Gotor[1]

[1]Instituto de Ciencia de Materiales de Sevilla (CSIC-US), Américo Vespucio 49, 41092 Sevilla, Spain.

[2]Departamento de Ingeniería Metalúrgica y de Materiales, Universidad Técnica Federico Santa María, Valparaíso 1680, Chile.

[3]Departamento de Química Inorgánica, Universidad de Sevilla (US), Calle Prof. García González 1, 41012, Sevilla, Spain.

ABSTRACT

The kinetics of the high-temperature oxidation of titanium-tantalum carbonitride-based cermets with different Ti/Ta ratios was studied. Isothermal oxidation tests were conducted under static air for 48 h at temperatures between 700ºC and 1200ºC. The oxidation satisfied the parabolic kinetics, characteristic of the existence of a protective oxide layer. The apparent activation energy suggests the rate-controlling process during oxidation is the simultaneous inward and outward diffusion of oxygen and titanium, respectively, through the formed protective layer, consisting mainly of a rutile phase. A higher Ta(V) content in the rutile decreased the oxygen diffusivity due to the reduction of oxygen vacancy concentration.

*Corresponding Author. Tel: +34 954489217. E-mail: ernesto.chicardi@icmse.csic.es

1. Introduction.

Cemented carbide cutting tools are widely used for room-temperature machining due to their exceptional toughness and damage tolerance under cyclic loading. However, they fail to meet the requirements for the most demanding processes, such as high-speed machining, due to their poor oxidation resistance at high temperatures (600–1000 °C), which can be reached on the tool/chip interface while in service [1-4]. At high temperature, wear diffusion plays an important role and is a limiting factor due to the increased reactivity between contact materials (tool and workpiece). If oxidation processes also occur, an additional wear mechanism is activated that can dramatically decrease the service life of the tool. To minimize these wear mechanisms, suitable coatings are required.

Cermets based on titanium carbonitride are powder-metallurgical composite materials that have drawn increasing attention in the machining industry [5-7], because their properties, such as high wear resistance, high chemical stability and good mechanical strength at high temperature, are well adapted to the requirements of specific machining processes such as high-speed finishing. The good mechanical performance of cermets at high temperature is also related to their good oxidation resistance. Especially promising is a new generation of cermets containing complex titanium-tantalum carbonitrides as the ceramic phase [8-12] that have been proven to possess outstanding oxidation resistance [13], satisfying the optimal requirements for many applications in the field of cutting tools.

Hot corrosion usually refers to phenomena involving chemical reactions at high temperature, typically when a gaseous phase (i.e. oxygen) produces extended damage to the material. Hot corrosion occurs, for example, when a material is allowed to react with air at high temperatures for a given time interval. The extent of the damage produced on the material will be a function of the kinetics of the gas/solid reaction under the given experimental conditions. In this light, hot corrosion that also includes oxidation is seen as a destructive process to be prevented for clear technological and economic reasons [5]. Kinetics analysis is an important aspect of the study of oxidation processes because it deals with the measurement and parameterization of the process rates. The goal of kinetics analysis is to obtain reliable kinetics parameters, i.e., the apparent activation energy (E_a), the pre-exponential factor (A) and the mechanism or kinetic model, to allow later prediction of the thermal stability of materials.

Although the oxidation kinetics of cemented carbides have been studied by some researchers [3, 14-20], published reports focusing on the oxidation kinetics of cermets are scarce [21, 22]. Given the high oxidation resistance of (Ti,Ta)(C,N)-based cermets, it is of considerable interest to perform a kinetics study using thermogravimetric measurements of the isothermal oxidation of this type of cermets in the temperature range of 700-1200ºC, covering the high-temperature range reached during the most demanding cutting operations.

2. Experimental methods.

A set of five cermets with nominal compositions of 80 wt% $Ti_xTa_{1-x}C_{0.5}N_{0.5}$ − 20 wt% Co and variable Ta content, x = 1, 0.99, 0.95, 0.90 and 0.80, were synthesized by the mechanochemical process termed Mechanically Induced Self-Sustaining Reaction (MSR) from Ti, Ta, C and Co powder mixtures and N_2 gas [23]. A powder mixture containing 46.5 g elemental Ti (99% purity, <325 mesh, Strem Chemicals), Ta (99.6% purity, <325 mesh, Alfa-Aesar), C (as graphite, <270 mesh, Fe < 0.4%, Merck) and Co (99.8% purity, <100 mesh, Strem Chemicals), together with 13 tempered steel balls (d = 20 mm, m = 32.6 g), were put into a tempered steel vial (300 ml in volume) and milled using a modified planetary ball mill (P4, Fritsch) at a spinning rate of 400 rpm under 6 atm N_2 gas (H_2O and O_2 < 3 ppm, Air Liquide). The planetary ball mill enabled the MSR reactions to be monitored by continuously measuring the pressure inside the vial [24]. When the MSR reaction associated with the synthesis of the $Ti_xTa_{1-x}C_{0.5}N_{0.5}$ carbonitride phase occurs, the temperature increases due to the release of heat from the exothermic formation reaction, which consequently increases the total pressure. The ignition time, defined as the critical milling time required to induce the MSR process, can then be determined from the spike in the recorded time-pressure data. After ignition, the milling is continued to ensure full conversion and homogenization. The ignition time was about 40-45 min for all cermets and the total milling time 75 min.

The powdered cermets synthesized by MSR were shaped using a uniaxial press (2 tons, 5 min) and compacted by cold isostatic pressing (200 MPa, 10 min). The green bodies were then sintered at temperatures between 1450ºC and 1550ºC, optimized for each Ta/Ti ratio [23], for 60 min under a flowing Ar (H_2O < 3 and O_2 < 2 ppm, Linde) atmosphere in a horizontal tubular furnace (IGM1360 model No. RTH-180-50-1H,

AGNI) to obtain cylindrical cermets 13 mm in diameter and 9 mm in height. After sintering, the cermets consisted of the mentioned carbonitride phase ($Ti_xTa_{1-x}C_{0.5}N_{0.5}$) and two Ti-Ta-Co intermetallic compounds, namely, (Ti_xTa_{1-x})Co_2 and (Ti_xTa_{1-x})Co, acting as binder instead of the initial Co. A complete study of phases and composition of cermets can be found in a previous work [23]. The cermets were labeled as **Ti100**, **Ti99Ta1**, **Ti95Ta5**, **Ti90Ta10** and **Ti80Ta20** according to the Ti and Ta atomic percent content in the ceramic carbonitride phase (x in $Ti_xTa_{1-x}C_{0.5}N_{0.5}$).

The oxidation experiments were performed on parallelepiped specimens of these five cermets with similar surface areas ($\sim 94\pm0.5$ mm^2). The specimens were obtained by cutting from the centers of the initial cylinders, and the surfaces were carefully prepared to reduce the flaws (e.g., pores, cracks) by successive grinding and polishing steps until a mirror effect was obtained. Three diamond discs with maximum diamond particle size of 60, 40 and 25 μm were used for grinding and diamond powder suspensions of 8, 4 and 1 μm for polishing.

The oxidation kinetics were studied based on thermogravimetric (TG) measurements using a CI Robal electrobalance (C.I. Electronics Ltd.) with a maximum weight allowed of 5 g and a sensitivity of 1 μg, which was attached to the support frame of a high-temperature vertical furnace (Severn Thermal Solutions Ltd, mod. SC448A). Specimens were placed on a platinum wire coil to maximize the contact of the surfaces with the surrounding atmosphere. The oxidations of the cermets were performed under isothermal conditions for 48 h in static air ($pO_2 \sim 0.21$ atm), at temperatures ranging from 700ºC to 1200ºC (heating rate of 20 ºC/min and free cooling). The cermets were also oxidized in air at 1300 ºC for the time necessary to achieve complete oxidation.

The polished cross sections of the oxidized parallelepipeds were examined by Scanning Electron Microscopy (SEM) performed on a Hitachi S-4800 SEM-FEG microscope coupled with an X-ray energy dispersive spectrometry (XEDS) detector (Quantax-EDS, Bruker Corporation). The SEM images obtained in secondary electron mode and XEDS-SEM mappings were used to observe the progress of oxidation and to determine the thickness of the oxide scale.

To inspect the possible appearance of liquid phase at the temperatures used in the oxidation study, Differential Scanning Calorimetry (DSC) measurements were

performed using a TA Instrument SDT Q600 with a constant heating rate of 10°C/min and a flowing helium atmosphere.

3. Results and discussion.

Figure 1 shows the evolution over time of the weight gain (in mg/cm^2) as a result of the oxidation of the different cermets for all of the temperatures studied. The expected increase in the extent of oxidation with temperature was observed for all of the cermets, as previously reported [25]. Moreover, Figure 1 clearly illustrates the benefit of the presence of Ta in improving the oxidation resistance of the cermets. For all temperatures, the weight gain continuously decreased as Ti was increasingly substituted for Ta in the cermets. Note that at 700ºC, the oxidation was undetectable for cermets with medium and high Ta content (**Ti95Ta5**, **Ti90Ta10** and **Ti80Ta20**). In contrast, at 1200ºC, the **Ti100** and **Ti99Ta1** cermets (cermets with low Ta content) reached complete oxidation before the end of the 48-h oxidation test. To highlight the improvement in the oxidation resistance of cermets as Ti is progressively replaced by Ta, the weight gain per unit area after 48 h of oxidation for all of the temperatures and cermets is shown in Figure 2a. Note, for example, that at 800ºC, the **Ti100** cermet exhibited an oxidation weight gain of 18.6 mg/cm^2, similar to the **Ti80Ta20** cermet, but at 1200ºC it was oxidized (19.7 mg/cm^2). Therefore, substituting 20 at% of Ti with Ta is as if oxidation were deferred by approximately 400ºC.

The outstanding decrease in the extent of oxidation with increasing Ta content in cermets was also clearly observed when the cross-sections of oxidized cermets were inspected by SEM after 48-h oxidation tests at different temperatures. The thickness of the region affected by oxidation was measured from the SEM images with the help of XEDS-SEM mappings, allowing the precise location of the interface between oxidized and unoxidized regions. The values are shown in Figure 2b, which are consistent with the thermogravimetric results of Figure 2a. Some examples of characteristic SEM images and XEDS-SEM mappings are shown in Figure 3, from which the effect of the Ta addition and the oxidation temperature on the extent of oxidation can also be determined.

As detailed in previous works [13, 26], phase identification by XRD and XEDS-SEM analyses showed for all of the cermets and temperatures that the oxide scale was dominated by the presence of rutile and the progression of the oxidation by the growth of the rutile layer, even though other Co-containing phases such as cobalt oxides (CoO and Co_3O_4) and cobalt titanates ($CoTiO_3$, Co_2TiO_4 and $CoTi_2O_5$) were also observed depending on the temperature and Ta content (Figure 4). For the cermets **Ti100** and **Ti99Ta1**, the formation in the oxide scale of a thin CoO/Co_3O_4 external layer was observed at low temperature that reacted with the underlying rutile phase to form cobalt titanates at increasing temperature. The disappearance of this CoO/Co_3O_4 external layer induced the emergence of the rutile phase at the surface of the oxide scale. For the cermets with higher Ta content (**Ti95Ta5**, **Ti90Ta10** and **Ti80Ta20**), the formation of a cobalt titanate external layer instead of the CoO/Co_3O_4 layer was observed at low temperature and remained stable and unaltered at increasing oxidation temperatures. Note that no open porosity was observed by SEM in the outer cobalt-rich layer, which was always highly compact. Although the rutile layer was relatively well-densified, large pores and/or voids were detected that were presumably generated by the coalescence of smaller ones formed because of the volatile species arising from the oxidation of the carbonitride phase. These species must remain partially occluded in these large pores. Moreover, below the compact oxide scale, an internal oxidation region composed of rutile and Co was also observed (Figure 5). Note that the thickness shown in Figure 2b comprises both the compact oxide scale and the internal oxidation region.

Figures 3a-f show good adhesion of the oxide scale, without any observed layer breakdown or spalling phenomena. The SEM images also revealed homogeneous oxidation of the cermets as the oxidation depth was similar on all sides of the specimens. Cermets maintained their original shape after the oxidation tests, and only an increase in volume was observed in agreement with the volume changes associated with oxidation. For example, the oxidation of the major carbonitride phase into rutile causes a volume increase of about 50%. The XRD diagrams of the fully oxidized specimens at 1300ºC revealed for all of them the presence of titanium-tantalum oxide with rutile structure ($Ti_xTa_{1-x}O_2$) and cobalt dititanate ($CoTi_2O_5$). Assuming $Ti_xTa_{1-x}O_2$ and $CoTi_2O_5$ to be the fully oxidized species, the relative weight balances associated with oxidation were calculated for each cermet and temperature and are shown in Figure

2c. An oxidation extent greater than 100% observed in those cermets with a higher degree of oxidation confirmed the fact that volatile species remained occluded in the closed porosity observed in SEM images (Figure 3a-f).

Figures 1 and 2 show the anomalous behavior at 1200ºC of the **Ti95Ta5** and **Ti90Ta10** cermets. A higher degree of oxidation than expected was observed for both cermets, as well as a linear oxidation behavior during approximately the first 6 h of oxidation (Figure 1). This behavior was attributed to the incipient formation of a liquid phase, corresponding to the partial melting of the intermetallic binder phase, according to the Ti-Co and Ta-Co binary phase diagrams [27]. Figure 6 shows the external surface of the **Ti95Ta5** cermet oxidized at 1200ºC, where a globular morphology characteristic of the appearance of a liquid phase can be observed. Moreover, the DSC curve of this cermet, shown in the inset of the Figure 6, revealed in this temperature range an endothermic peak associated with the formation of a liquid phase. The presence of this liquid phase could facilitate oxygen diffusion into the cermets, resulting in increased oxidation. In the **Ti80Ta20** cermet, this anomalous behavior was not observed due to the higher Ta content, which induces a higher melting point in the intermetallic binder phase.

3.1. Oxidation kinetics.

The thermogravimetric curves in Figure 1 reveal that for all of the different cermets and temperatures, the oxidation rate tended to decrease with time. This evolution can be successfully fitted (Figure 1) according to the following general kinetics equation (1):

$$\left(\frac{\Delta m}{s}\right) = k_n t^n + C \qquad (1)$$

where Δm is the weight gain; s is the cermet surface area; t is the oxidation time; k_n is the oxidation rate constant; n is the oxidation exponent; and C is a constant that includes the oxidation prior to reaching the isothermal condition.

The values of n determined by fitting the experimental data using equation (1) are shown in Table 1 along with the coefficient of determination (R^2) as an indication of the goodness of fit. The n values obtained are in most of cases in the range 0.4-0.6, fully compatible with parabolic oxidation kinetics ($n = 0.5$). A larger deviation from

parabolic behavior was observed in the **Ti95Ta5** and **Ti90Ta10** cermets oxidized at 1200ºC, due, as mentioned above, to the presence of a liquid phase, which tends to accelerate the oxidation.

Linear, logarithmic and parabolic kinetics are simple models that try to explain the oxidation behavior of pure metals. When a pure metal is exposed to oxidation, the resulting oxide layer generally covers the metal surface. Linear oxidation kinetics, corresponding to $n = 1$ in equation (1), involve the formation of a non-protective oxide layer because of, for example, the presence of pores or cracks in the layer or volatile oxide products. In this case, the metal is permanently in contact with oxygen, and the oxide layer growth (or metal oxidation rate) is constant over oxidation time and independent of its thickness. The oxidation progress is independent of the amount of gas or metal previously consumed in the reaction and the oxidation rate is controlled by the chemical reaction itself.

In contrast, parabolic oxidation kinetics ($n = 0.5$ in equation (1)) imply the formation of a protective oxide layer whose growth rate is inversely proportional to its thickness; that is, the growth rate of the protective layer decreases with the oxidation time. Parabolic kinetics assume a diffusion-controlled process in which diffusion through the oxide layer of oxygen to the oxide/substrate interface or of metal to the oxygen/oxide interface is the rate-limiting oxidation process. It is also assumed that the concentration of reactive species at each boundary of the oxide layer is constant. Finally, logarithmic oxidation kinetics usually occur at low oxidation temperatures and are characterized by the formation of a thin oxide layer whose growth rate quickly decelerates, giving rise to a passivation phenomenon.

Although previously oxidation studies typically report on more complex systems than pure metals [28-30], where even selective oxidation phenomena are observed [31], quasi-parabolic kinetic behavior (n values slightly different from 0.5) is often observed [32-34]. Deviations are common because even ideal models cannot perfectly describe real situations, in which fast diffusion paths at localized positions, such as grain boundaries or lattice defects or other factors, simultaneously influence the oxidation process. Nevertheless, quasi-parabolic kinetics is always associated with the existence of a protective oxide layer.

Therefore, the parabolic kinetics observed in the oxidation of cermets, supported by the good linearity of the plot of the *specific weight gain vs. $t^{0.5}$* (Figure 7), clearly indicate the formation of a compact and continuous oxide layer on the surface of the cermets, as shown for example in Figure 4 for cermets **Ti99Ta1** and **Ti95Ta5** oxidized at 800ºC and 1100ºC, respectively. Note that the plots corresponding to the highest tested oxidation temperature for each cermet are not presented in Figure 7 due to poor linearity, most likely as a consequence of the aforementioned partial melting of the binder phase.

The parabolic rate constant, k_p, for each temperature and cermet was calculated from the slope of the linear fittings in Figure 7, and the values are shown in Table 2. It can be clearly observed how the parabolic rate constant for the same oxidation temperature depends strongly on the Ta content. This result corroborates the effectiveness of Ta addition in improving the oxidation resistance of cermets. As an example, k_p for the **Ti100** cermet at each temperature is approximately two and three orders of magnitude higher than for the **Ti95Ta5** and **Ti80Ta20** cermets, respectively.

Moreover, as for any thermally activated kinetic process, the values of k_p (Table 2) reveal a strong influence of temperature, increasing by approximately a factor of ten every 100ºC. This dependence of k_p on the oxidation temperature can be expressed by the Arrhenius equation (2) [35]:

$$k_p = Ae^{\left(-E_a/R\cdot T\right)} \qquad (2)$$

where A is the pre-exponential or frequency factor; E_a is the apparent activation energy; R is the universal gas constant; and T is the absolute temperature.

The apparent activation energy of the oxidation process was calculated from the slope of the plot of *$ln(k_p)$ vs. $1/T$* (Figure 8), and the values obtained are shown in Table 3. The E_a values found for cermets containing Ta (cermets **Ti99Ta1**, **Ti95Ta5**, **Ti90Ta10** and **Ti80Ta20**) were in the range 225-256 kJ mol^{-1}, in close agreement with the values reported in the literature for the activation energy of both the self-diffusion of oxygen and titanium in rutile, which have similar values [36-38]. Rutile generally exhibits significant non-stoichiometry, and the oxygen deficiency appears to be accommodated by oxygen vacancies and Ti interstitials, with oxygen vacancies

dominating at high temperatures and relatively oxidizing conditions, and Ti interstitials at lower temperatures and more reducing conditions. These point defects have an important influence on diffusion, with oxygen vacancies promoting oxygen diffusion, and Ti interstitials promoting the diffusion of titanium. Despite the experimental conditions used (high temperature and high oxidizing atmosphere) and the fact that oxygen vacancy is a lower-energy defect, Ti and O diffusions can be competitive processes as Ti interstitials possess a lower migration barrier [39]. Note that at the oxide/cermet interface the oxygen partial pressure must be significantly lower than at the air/oxide interface and then the defect structure can change through the oxide scale.

The existence of an internal oxidation region, in which rutile and Co coexist (Figure 5), was a clear evidence that oxidation had taken place at the oxide/cermet interface (away from the cermet surface), which implies the inward diffusion of oxygen. However, XEDS-SEM measurements in the rutile layer revealed the existence of a chemical gradient in the $Ti_xTa_{1-x}O_2$ solid solution. No Ta was observed near the surface, while moving inwards, the amount of Ta increased in the rutile phase. These results suggest that the rutile layer also grew due to the outward diffusion of Ti. Therefore, the diffusion-controlled process of the long-term oxidation of cermets should include both the inward diffusion of oxygen and the outward diffusion of titanium through the rutile layer formed, independent of the Ta content. The lower value (182 kJ mol^{-1}) obtained for the **Ti100** cermet must be related to the presence of a greater proportion of porosity and voids, which can create shortcuts for the oxygen pathway to the oxide/cermet interface.

Even though the presence of Ta does not seem to modify the temperature dependence of the oxidation, the Ta amount introduced in cermets plays an important role in reducing the oxidation rate, as observed in related systems such as Ti-Ta alloys, $Ta_xTi_{1-x}C$ and $Ta_xTi_{1-x}C_yN_{1-y}$ whiskers and $TiC_{0.5}N_{0.5}$-10 mol% TaC ceramics [20, 29, 40, 41]. Although it has been proven that the introduction of Ta(V) in the rutile structure leads to the formation of Ti(III) in one of the nearest-neighbor cation sites [42] it has also been shown that Ta doping reduces the oxygen mobility [43], which should probably be due to a reduction in the concentration of oxygen vacancies. Therefore, by increasing Ta content in cermets, the rutile phase resulting from oxidation possesses a higher abundance of Ta(V), which would be expected to lower oxygen diffusivity [37]. Note that when Ta was introduced into cermets, a significant reduction of the internal

degradation zone was observed, which agrees with a reduced availability of oxygen at the oxide/cermet interface.

4. Conclusions.

1. The oxidation of $Ti_xTa_{1-x}C_{0.5}N_{0.5}$-Co-based cermets with different Ta contents was studied in static air at temperatures between 700ºC and 1200ºC.

2. It was determined that the oxidation kinetics satisfied the parabolic kinetic law for all cermets and temperatures, which is characteristic of the presence of a protective oxide layer.

3. The calculated apparent activation energy suggests that the oxidation rate is controlled by the inward oxygen diffusion and the outward titanium diffusion through the formed rutile layer.

4. The remarkable improvement of the oxidation resistance with an increase in Ta content is the result of the replacement of Ti^{4+} by Ta^{5+} in the rutile structure, which reduces the concentration of oxygen vacancies and, consequently, the oxygen mobility and the inward oxygen diffusivity.

References.

[1] S.N. Basu, V.K. Sarin, Oxidation behavior of WC-Co, Materials Science and Engineering a-Structural Materials Properties Microstructure and Processing, 209 (1996) 206-212.
[2] S.K. Bhaumik, R. Balasubramaniam, G.S. Upadhyaya, M.L. Vaidya, Oxidation behavior of hard and binder phase modified WC-10Co cemented carbides, Journal of Materials Science Letters, 11 (1992) 1457-1459.

[3] B. Casas, X. Ramis, M. Anglada, J.M. Salla, L. Llanes, Oxidation-induced strength degradation of WC-Co hardmetals, Int. J. Refract. Met. Hard Mat., 19 (2001) 303-309.

[4] L. Chen, D. Yi, B. Wang, H. Liu, C. Wu, X. Huang, H. Li, Y. Gao, The selective oxidation behaviour of WC–Co cemented carbides during the early oxidation stage, Corrosion Science, 94 (2015) 1-5.

[5] P. Ettmayer, H. Kolaska, W. Lengauer, K. Dreyer, Ti(C,N) Cermets - Metallurgy and Properties, International Journal of Refractory Metals and Hard Materials, 13 (1995) 343.

[6] L. Chen, W. Lengauer, K. Dreyer, Advances in modern nitrogen-containing hardmetals and cermets, International Journal of Refractory Metals and Hard Materials, 18 (2000) 153-161.

[7] J.H. Perepezko, J.M. Bero, R. Sakidja, I.G. Talmy, J. Zaykoski, Oxidation resistant coatings for refractory metal cermets, Surface & Coatings Technology, 206 (2012) 3816-3822.

[8] E. Chicardi, J.M. Córdoba, M.J. Sayagués, F.J. Gotor, Absence of the core-rim microstructure in TixTa1-XCyN1-y-based cermets developed from a pre-sintered carbonitride master alloy, International Journal of Refractory Metals and Hard Materials, 33 (2012) 38-43.

[9] E. Chicardi, J.M. Córdoba, M.J. Sayagués, F.J. Gotor, Inverse core-rim microstructure in (Ti,Ta)(C,N)-based cermets developed by a mechanically induced self-sustaining reaction, International Journal of Refractory Metals and Hard Materials, 31 (2012) 39-46.

[10] J.M. Córdoba, M.A. Avilés, M.J. Sayagués, M.D. Alcalá, F.J. Gotor, Synthesis of complex carbonitride powders TiyMT1-yCxN1-x (MT:Zr,V,Ta,Hf) via a mechanically induced self-sustaining reaction, Journal of Alloys and Compounds, 482 (2009) 349-355.

[11] J.M. Cordoba, E. Chicardi, R. Poyato, F.J. Gotor, V. Medri, S. Guicciardi, C. Melandri, Spark plasma sintering of TixTa1-xC0.5N0.5-based cermets: Effects of processing conditions on chemistry, microstructure and mechanical properties, Chemical Engineering Journal, 230 (2013) 558-566.

[12] E. Chicardi, Y. Torres, M.J. Sayagues, V. Medri, C. Melandri, J.M. Cordoba, F.J. Gotor, Toughening of complete solid solution cermets by graphite addition, Chemical Engineering Journal, 267 (2015) 297-305.

[13] E. Chicardi, F.J. Gotor, J.M. Cordoba, Enhanced oxidation resistance of Ti(C,N)-based cermets containing Ta, Corrosion Science, 84 (2014) 11-20.

[14] L. del Campo, R.B. Perez-Saez, L. Gonzalez-Fernandez, M.J. Tello, Kinetics inversion in isothermal oxidation of uncoated WC-based carbides between 450 and 800 degrees C, Corrosion Science, 51 (2009) 707-712.

[15] C. Barbatti, J. Garcia, P. Brito, A.R. Pyzalla, Influence of WC replacement by TiC and (Ta,Nb)C on the oxidation resistance of Co-based cemented carbides, Int. J. Refract. Met. Hard Mat., 27 (2009) 768-776.

[16] M. Aristizabal, J.M. Sanchez, N. Rodriguez, F. Ibarreta, R. Martinez, Comparison of the oxidation behaviour of WC-Co and WC-Ni-Co-Cr cemented carbides, Corrosion Science, 53 (2011) 2754-2760.

[17] X. Chen, H. Liu, Q. Guo, S. Sun, Oxidation behavior of WC-Co hard metal with designed multilayer coatings by CVD, Int. J. Refract. Met. Hard Mat., 31 (2012) 171-178.

[18] L. Chen, B. Wang, D. Yi, H. Liu, Non-isothermal oxidation kinetics of WC-6Co cemented carbides in air, Int. J. Refract. Met. Hard Mat., 40 (2013) 19-23.

[19] S.T. Aly, S.K. Amin, S.A. El Sherbiny, M.F. Abadir, Kinetics of isothermal oxidation of WC-20Co hot-pressed compacts in air, Journal of Thermal Analysis and Calorimetry, 118 (2014) 1543-1549.

[20] D.S. Park, C. Park, Y.D. Lee, Oxidation of Ti(C,N)-based ceramics exposed at 1373 K in air, Journal of the American Ceramic Society, 83 (2000) 672-674.

[21] F. Monteverde, A. Bellosi, Oxidation behavior of titanium carbonitride based materials, Corrosion Science, 44 (2002) 1967-1982.

[22] P. Alvaredo, C. Abajo, S.A. Tsipas, E. Gordo, Influence of heat treatment on the high temperature oxidation mechanisms of an Fe-TiCN cermet, Journal of Alloys and Compounds, 591 (2014) 72-79.

[23] E. Chicardi, Y. Torres, J.M. Cordoba, P. Hvizdos, F.J. Gotor, Effect of tantalum content on the microstructure and mechanical behavior of cermets based on (TixTa1-x)(C0.5N0.5) solid solutions, Materials & Design, 53 (2014) 435-444.

[24] C. Suryanarayana, Mechanical alloying and milling, Progress in Materials Science, 46 (2001) 1-184.

[25] Q. Yang, W. Xiong, S. Li, Z. Yao, X. Chen, Early high temperature oxidation behaviour of Ti(C,N)-based cermets in air, Corrosion Science, 52 (2010) 3205-3211.

[26] E. Chicardi, F.J. Gotor, J.M. Cordoba, High temperature oxidation resistance of (Ti,Ta)(C,N)-based cermets, Corrosion Science, (Under review).

[27] O.H. Baker H, Alloy Phase Diagrams, ASM Handbook, 1992.

[28] F. Gesmundo, B. Gleeson, Oxidation of multicomponent 2-phase alloys, Oxidation of Metals, 44 (1995) 211-237.

[29] Y. Park, D.P. Butt, Composition dependence of the kinetics and mechanisms of thermal oxidation of titanium-tantalum alloys, Oxidation of Metals, 51 (1999) 383-402.

[30] S. Ningshen, U.K. Mudali, P. Mukherjee, A. Sarkar, P. Barat, N. Padhy, B. Raj, Influence of oxygen ion irradiation on the corrosion aspects of Ti-5%Ta-2%Nb alloy and oxide coated titanium, Corrosion Science, 50 (2008) 2124-2134.

[31] D.J. Young, B. Gleeson, Alloy phase transformations driven by high temperature corrosion processes, Corrosion Science, 44 (2002) 345-357.

[32] E. Butchereit, K.G. Nickel, A. Muller, Precursor-derived Si-B-C-N ceramics: Oxidation kinetics, Journal of the American Ceramic Society, 84 (2001) 2184-2188.

[33] N. Babu, R. Balasubramaniam, A. Ghosh, High-temperature oxidation of Fe3Al-based iron aluminides in oxygen, Corrosion Science, 43 (2001) 2239-2254.

[34] D. Yao, R. Cai, C. Zhou, J. Sha, H. Jiang, Experimental study and modeling of high temperature oxidation of Nb-base in situ composites, Corrosion Science, 51 (2009) 364-370.

[35] K.J. Laidler, Chemical Kinetics, 3rd. ed., Harper and Row, New York, 1987.

[36] D.K. Moore, D.J. Cherniak, E.B. Watson, Oxygen diffusion in rutile from 750 to 1000 degrees C and 0.1 to 1000 MPa, American Mineralogist, 83 (1998) 700-711.

[37] J.A. Van Orman, L.K. Crispin, Diffusion in Oxides Mineralogical Society of America, USA, 2010.

[38] K. Hoshino, N.L. Peterson, C.L. Wiley, Diffusion and point-defects in TiO2-x, Journal of Physics and Chemistry of Solids, 46 (1985) 1397-1411.

[39] H. Iddir, S. Ogut, P. Zapol, N.D. Browning, Diffusion mechanisms of native point defects in rutile TiO2: Ab initio total-energy calculations, Physical Review B, 75 (2007).

[40] N. Ahlen, M. Johnsson, M. Nygren, Oxidation behaviour of TaxTi1-xC and TaxTi1-xCyN1-y whiskers, Thermochim. Acta, 336 (1999) 111-120.

[41] S. Shimada, Y. Seki, M. Johnsson, Thermoanalytical study on oxidation of TixTa1-xCyN1-y whiskers with formation of carbon, Solid State Ion., 167 (2004) 407-412.

[42] B.J. Morgan, D.O. Scanlon, G.W. Watson, Small polarons in Nb- and Ta-doped rutile and anatase TiO2, Journal of Materials Chemistry, 19 (2009) 5175-5178.

[43] V. Guidi, M.C. Carotta, M. Ferroni, G. Martinelli, M. Sacerdoti, Effect of dopants on grain coalescence and oxygen mobility in nanostructured titania anatase and rutile, Journal of Physical Chemistry B, 107 (2003) 120-124.

Figure captions.

Figure 1. The evolution of the weight gain per unit area (mg/cm^2) over time during the oxidation tests in static air for cermets **Ti100**, **Ti99Ta1**, **Ti95Ta5**, **Ti90Ta10** and **Ti80Ta20** at different oxidation temperatures: a) 700ºC; b) 800ºC; c) 900ºC; d) 1000ºC; e) 1100ºC; f) 1200ºC. Points: experimental data. Lines: fitted using equation (1).

Figure 2. Specific weight change (mg/cm^2) (a) and thickness of the area affected by oxidation (b) *vs.* temperature for cermets **Ti100**, **Ti99Ta1**, **Ti95Ta5**, **Ti90Ta10** and **Ti80Ta20** at oxidation temperatures between 700ºC and 1200ºC after the 48-h oxidation tests.

Figure 3. Secondary SEM images showing the effect of oxidizing temperature (cermet **Ti100** at 700ºC (a), 900ºC (b) and 1000ºC (c)) and Ta content (cermets **Ti95Ta5** (d), **Ti90Ta10** (e) and **Ti80Ta20** (f) oxidized at 1200ºC) on the thickness of the oxidized zone. (g-h) Oxygen XEDS-SEM mapping showing the interface between oxidized and unoxidized cermet.

Figure 4. Secondary SEM images of cermets **Ti99Ta1** (a) and **Ti95Ta5** (b) oxidized at 800ºC, showing the outer layer of cobalt oxide and cobalt titanate, respectively, and the compact and continuous rutile layer. Inset: The same cermets **Ti99Ta1** (a) and **Ti95Ta5** (b) oxidized at higher temperature (1100ºC) showing the disappearance of the cobalt oxide layer and the maintaining of the cobalt titanate layer, respectively.

Figure 5. XEDS-SEM mappings of the internal oxidation region in cermet **Ti95Ta5** oxidized at 1200ºC, showing the complete oxidation of the carbonitride phase and the partial oxidation of the binder phase. Elements: Green (O), blue (Co), red (Ti) and yellow (Ta).

Figure 6. Secondary SEM image of the external surface of **Ti95Ta5** cermet oxidized at 1200ºC. Inset: DSC curve of this cermet showing an endothermic peak associated with the formation of a liquid phase.

Figure 7. Linear plot of the parabolic oxidation kinetics (weight gain per unit area (mg/cm^2) *vs.* t^n, with n = 0.5) for cermets **Ti100** and **Ti99Ta1** in the temperature range of 700ºC-1000ºC and for cermets **Ti95Ta5**, **Ti90Ta10** and **Ti80Ta20** between 800ºC and 1100ºC.

Figure 8. Arrhenius plots corresponding to the dependence of the parabolic rate constant on temperature for the five cermets: **Ti100, Ti99Ta1, Ti95Ta5**, **Ti90Ta10** and **Ti80Ta20** at oxidation temperature between 700ºC and 1100ºC.

Table 1. Values of the oxidation exponent (n) and coefficient of determination (R^2) obtained by fitting the curves shown in figure 1 using equation (1) for cermets **Ti100**, **Ti99Ta1**, **Ti95Ta5**, **Ti90Ta10** and **Ti80Ta20** at oxidation temperatures between 700ºC and 1200ºC.

T (ºC)	Cermet				
	Ti100	**Ti99Ta1**	**Ti95Ta5**	**Ti90Ta10**	**Ti80Ta20**
	n (R^2)	**n (R^2)**	**n (R^2)**	**n (R^2)**	**n (R^2)**
700	0.61 (0.999)	0.41 (0.994)	-	-	-
800	0.57 (0.999)	0.47 (0.999)	0.43 (0.990)	0.39 (0.996)	0.41 (0.965)
900	0.57 (0.999)	0.58 (0.999)	0.47 (0.997)	0.47 (0.998)	0.50 (0.965)
1000	0.54 (0.996)	0.57 (0.999)	0.61 (0.999)	0.50 (0.999)	0.52 (0.997)
1100	0.40 (0.984)	0.43 (0.999)	0.55 (0.999)	0.58 (0.999)	0.51 (0.999)
1200	-	-	0.28 (0.929)	0.30 (0.960)	0.37 (0.989)

Table 2. Values of the parabolic rate constant (k_p) obtained from the slope of the linear fitting in figure 7 and the coefficient of determination (r) for cermets **Ti100**, **Ti99Ta1**, **Ti95Ta5**, **Ti90Ta10** and **Ti80Ta20** at oxidation temperatures between 700ºC and 1200ºC.

Cermet	T_{ox} (ºC)	k_p (mg^2 cm^{-4} s^{-1})	r
Ti100	**700**	2.30 x 10^{-4}	0.998
	800	2.22 x 10^{-3}	0.999
	900	1.44 x 10^{-2}	0.999
	1000	4.22 x 10^{-2}	0.999
Ti99Ta1	**700**	1.72 x 10^{-5}	0.997
	800	1.78 x 10^{-4}	0.999
	900	1.45 x 10^{-3}	0.998
	1000	1.29 x 10^{-2}	0.999
Ti95Ta5	**800**	2.14 x 10^{-5}	0.992
	900	9.55 x 10^{-5}	0.999
	1000	9.16 x 10^{-4}	0.998
	1100	7.83 x 10^{-3}	0.999
Ti90Ta10	**800**	4.45 x 10^{-6}	0.998
	900	3.68 x 10^{-5}	0.999
	1000	3.88 x 10^{-4}	0.999
	1100	2.19 x 10^{-3}	0.999
Ti80Ta20	**800**	1.93 x10^{-6}	0.982
	900	1.49 x 10^{-5}	0.997
	1000	1.16 x 10^{-4}	0.998
	1100	4.57 x 10^{-4}	0.999

Table 3. Apparent activation energy (E_a) determined for the oxidation process from the Arrhenius equation (2) and the coefficient of determination (r) for cermets **Ti100**, **Ti99Ta1**, **Ti95Ta5**, **Ti90Ta10** and **Ti80Ta20**.

Cermet	E_a (kJ mol^{-1})	r
Ti100	182 ± 10	0.9971
Ti99Ta1	225 ± 10	0.9979
Ti95Ta5	242 ± 17	0.9882
Ti90Ta10	256 ± 10	0.9985
Ti80Ta20	226 ± 7	0.9991

Figure 1

Figure 2

a) Ti100_700°C — 63 μm — 100 μm

d) Ti95Ta5_1200°C — 999 μm — 500 μm

b) Ti100_900°C — 584 μm — 500 μm

e) Ti90Ta10_1200°C — 749 μm — 500 μm

c) Ti100_1000°C — 1331 μm — 500 μm

f) Ti80Ta20_1200°C — 261 μm — 200 μm

g) Map data 4142 — MAG: 2000 x HV: 10.0 kV WD: 14.9 mm — 10 μm

h) Oxygen — Map data 4142 — MAG: 2000 x HV: 10.0 kV WD: 14.9 mm — 10 μm
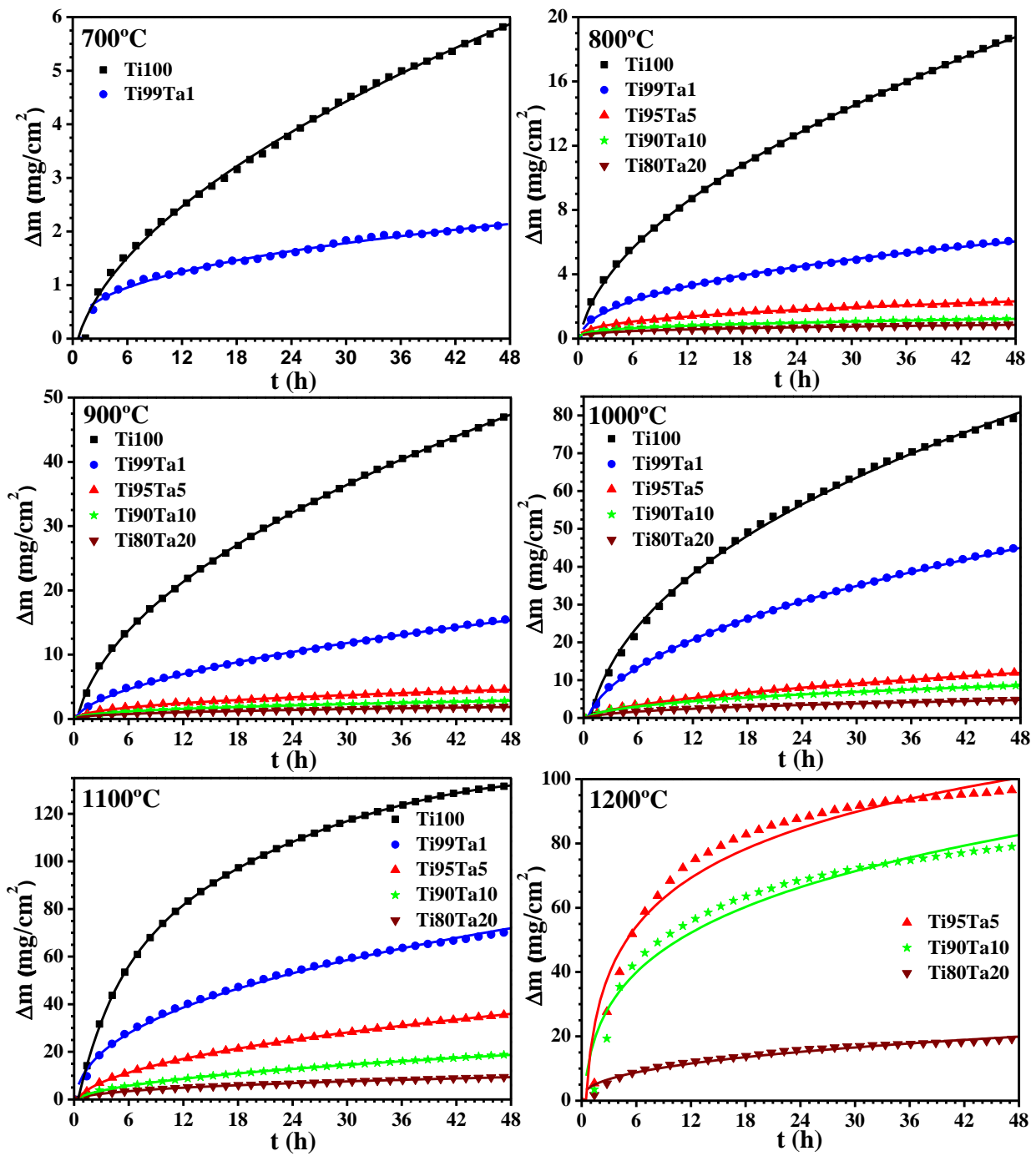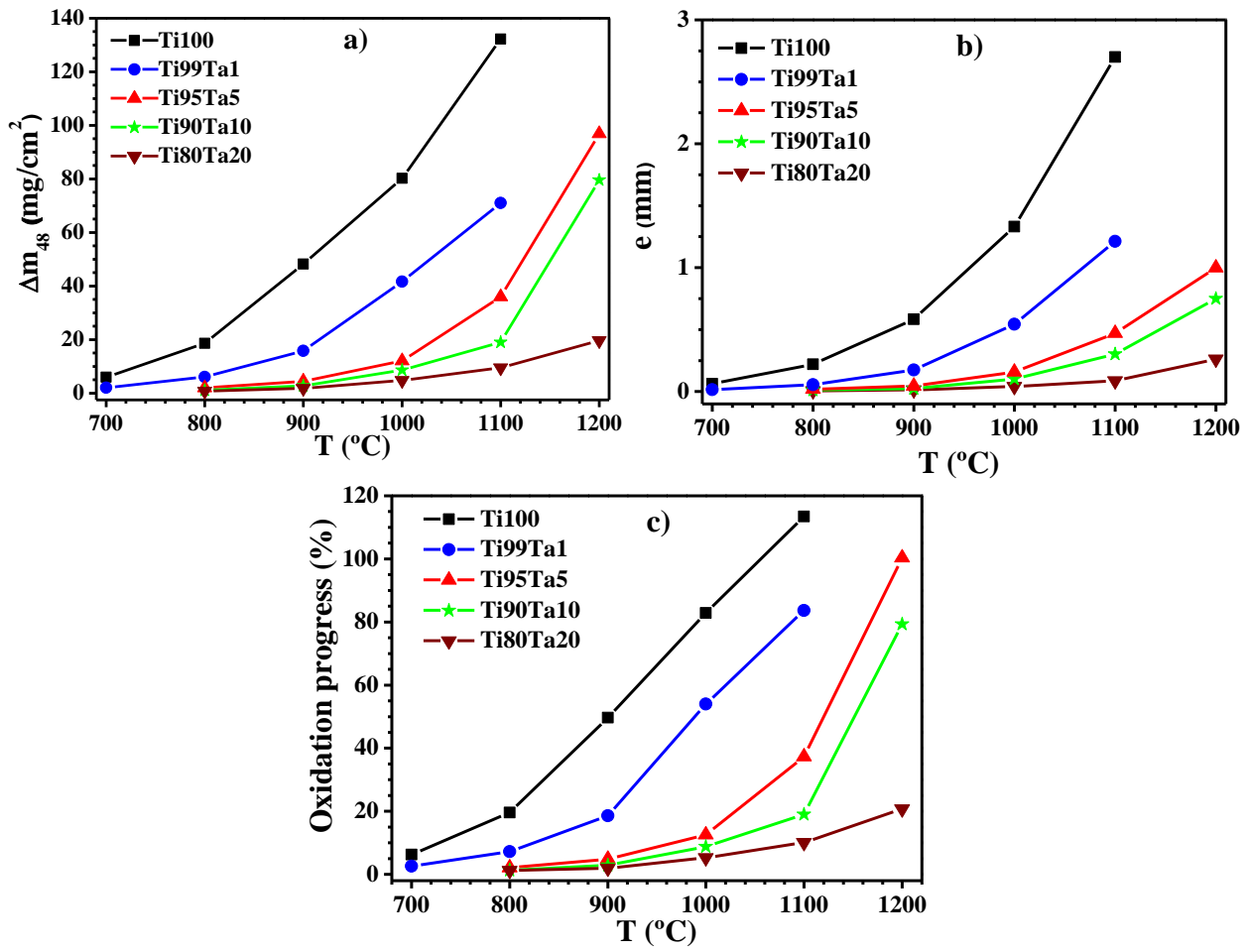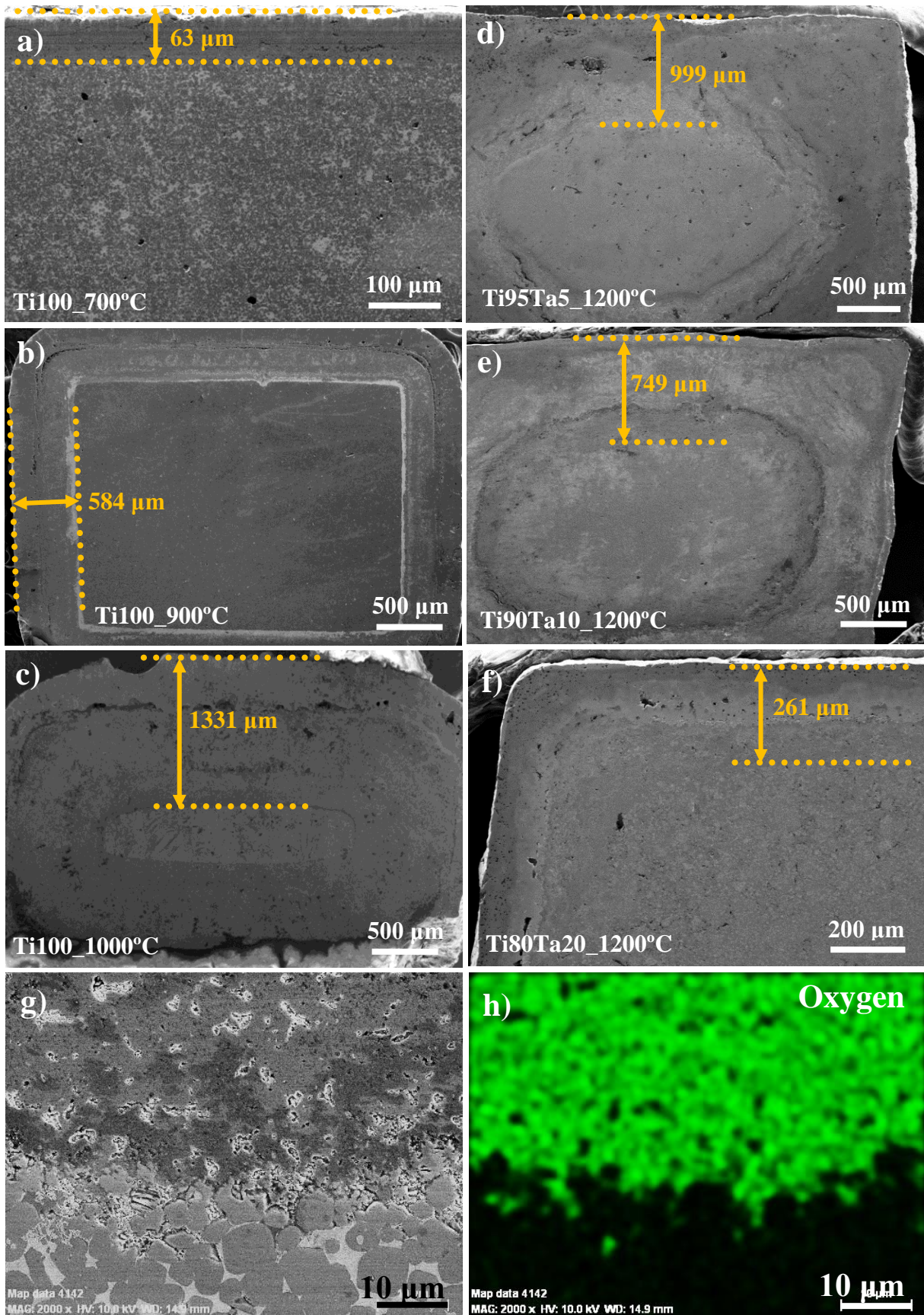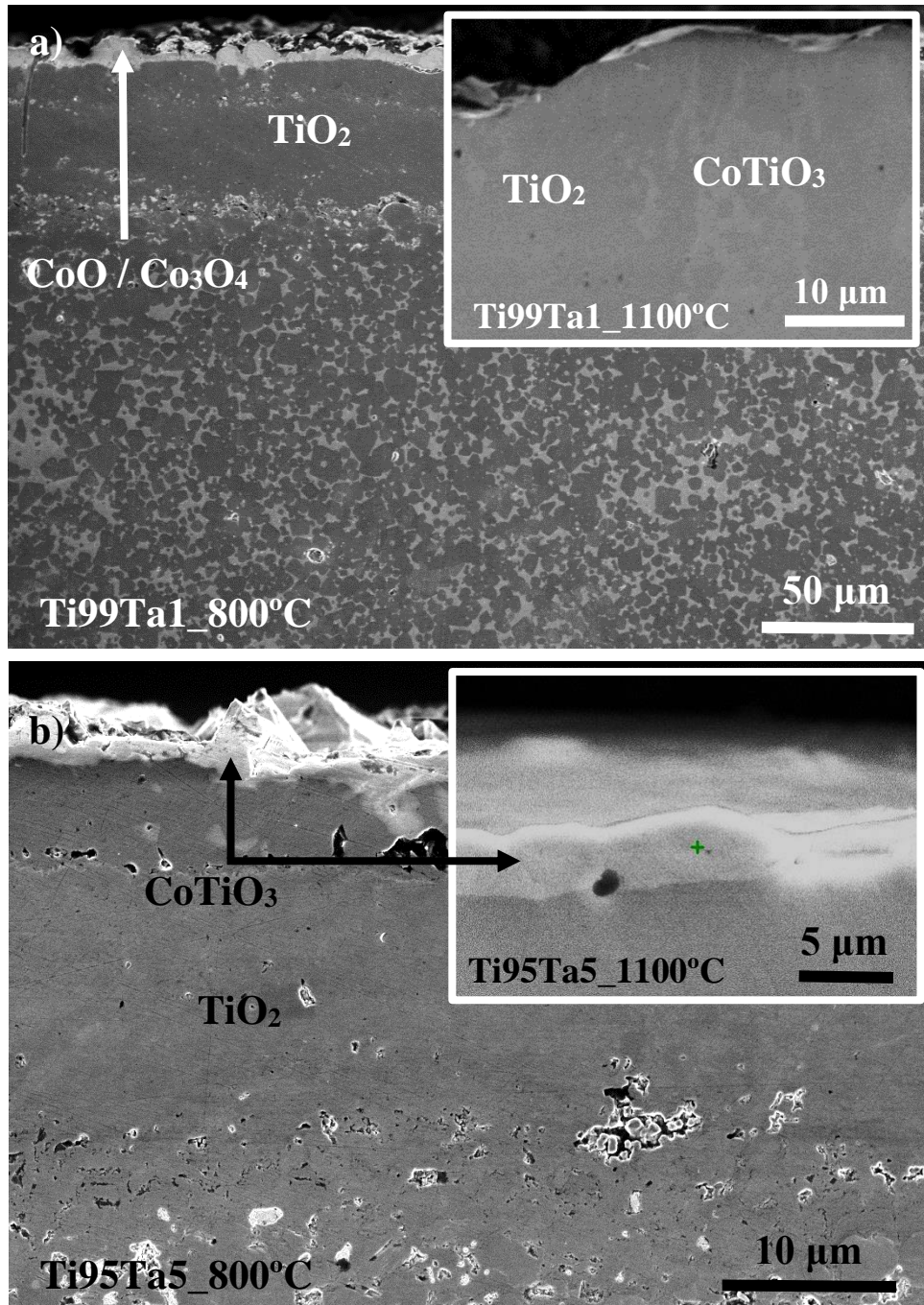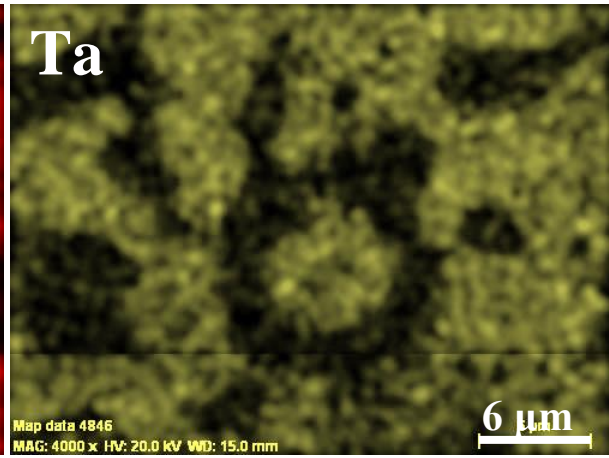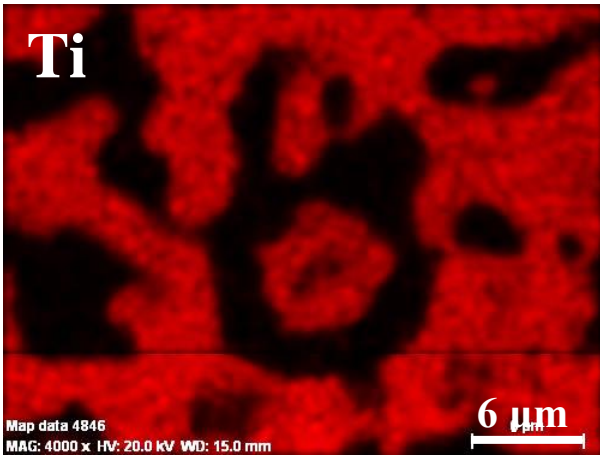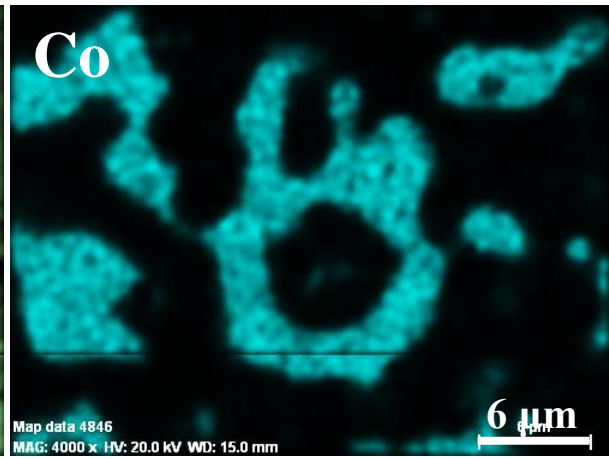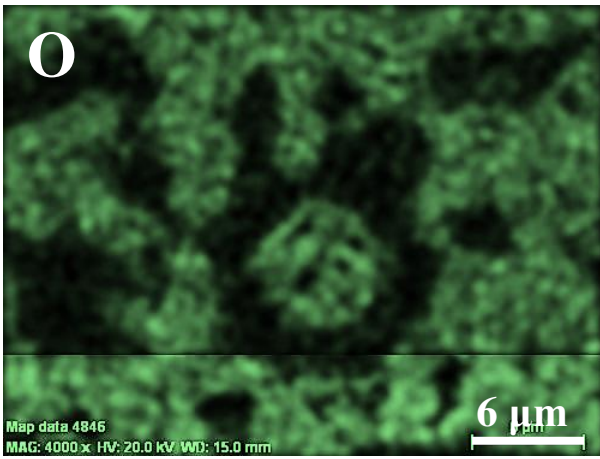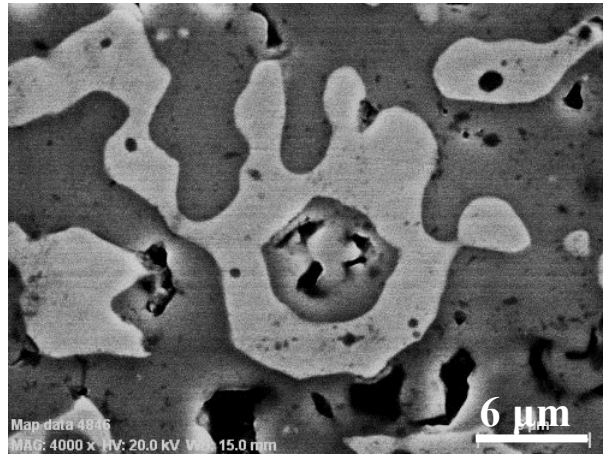
Figure 3

Figure 4

Figure 5
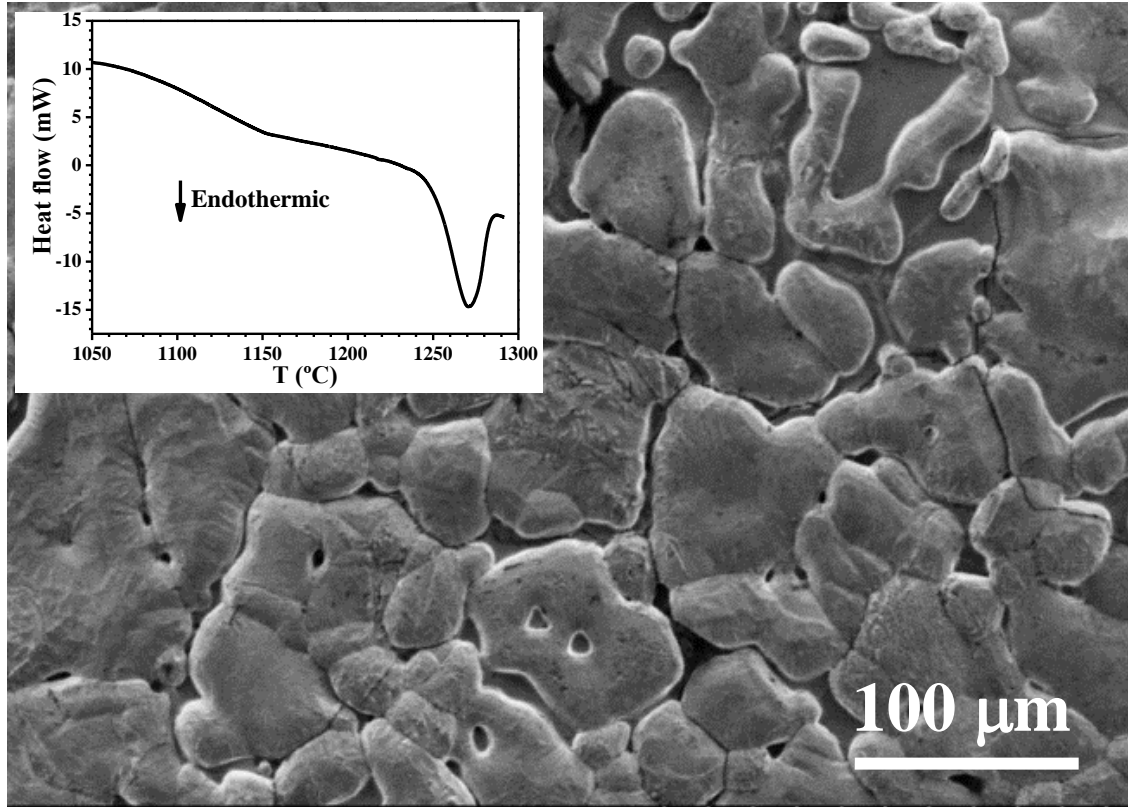
Figure 6

Figure 7

Figure 8